Kinematic analyses of brittle roto-translational planar and listric faults based on various rotational to translational velocities of the faulted blocks

Article *in* Marine and Petroleum Geology · April 2019

DOI: 10.1016/j.marpetgeo.2019.04.024

CITATION
1

READS
126

2 authors:

Soumyajit Mukherjee
Indian Institute of Technology Bombay
224 PUBLICATIONS **2,464** CITATIONS

SEE PROFILE

Lokesh Tayade
Indian Institute of Science Education and Research, Pune
1 PUBLICATION **1** CITATION

SEE PROFILE

Marine and Petroleum Geology 107 (2019) 326–333

Contents lists available at ScienceDirect

Marine and Petroleum Geology

journal homepage: www.elsevier.com/locate/marpetgeo

Research paper

Kinematic analyses of brittle roto-translational planar and listric faults based on various rotational to translational velocities of the faulted blocks

Soumyajit Mukherjee[a,*], Lokesh Tayade[b]

[a] Department of Earth Sciences, Indian Institute of Technology Bombay, Powai, Mumbai, 400 076, Maharashtra, India
[b] Department of Earth and Climate Science, Indian Institute of Science Education and Research Pune, Dr. Homi Bhabha Road, Pashan, Pune, 411 008, Maharashtra, India

ARTICLE INFO

Keywords:
Tribology
Translation with rotation
Deformation mechanism
Deformation kinematics
Brittle slip
Geomodeling

ABSTRACT

Research on rotational/roto-translational faults have been relatively less than translational faults. This is despite perfect translational faults seldom occur in mega-scale. This work models slickenside lineation patterns on planar and listric fault planes for different ratios of rates of rotation to the uniform speed towards a specific geographic direction ("ω/v") of faulted blocks. Curves simulated for the planar fault planes are fitted with natural examples of such roto-translational faults. In our 10 chosen examples, the "ω/v" ratio ranges between 0.2 (fault at San Miguelito range, Central México) and as high as 2.4 (fault at Hyogoken-Nambu, Japan). Knowing the "ω/v" ratios from terrains can better interpret its tectonics, For example, if "v" and the total time of duration of the deformation are known from some other studies, even the total amount of rotation can be estimated. The far-reaching implication of this study is that, as several hydrocarbon reserves and terrains with landslides are related to roto-translational faults, this work will be a stepping-stone in petroleum geosciences (e.g., stability of hydercarbon reserve) and engineering geology (e.g., stability of slope).

1. Introduction

Deciphering kinematics of faulting is one of the fundamental exercises in structural geology (e.g., Rowland and Sibson, 2001). Having diverse geometries, slickensides may develop on fault planes indicating either 180° apart two possible directions or a unique direction of slip (Doblas et al., 1997, Doblas, 1998; Mukherjee, 2014, 2015; Dasgupta and Mukherjee, 2017).

In nature/ in meso-scale/ in field, purely translational faults (Fig. 1a) with perfectly straight slickensides are found rarely. A true rotational fault (Fig. 1.b1) has also not yet been reported in the geoscience literature. Natural slickensides, on the other hand, are usually gently to moderately curved. This indicates that the faulted blocks rotate to some amount when they translate (review in Mukherjee and Khonsari, 2017). Such lineations indicate neither a first translation followed by rotation nor a vice versa, as in those cases two distinct lineation patterns would have developed one perfectly linear and another perfectly circular. Only in cases of ideal dip slip and strike slip book-shelf gliding (Mukherjee, 2018; Mukherjee and Khonsari, 2018), significantly rotated crustal blocks can leave straight slickensides at the fault surface i.e., at the interfaces between the two books/crustal blocks.

Mandal and Chakraborty (1989) refer the natural faults with simultaneous rotation and translation as the roto-translational faults (Fig. 1c). Rep. Fig. 1 presents the global distribution of such faults where curved slickensides have been noted/photographed by the previous authors. Few papers on theoretical analyses of rotational fault kinematics based on tangent lineation diagrams using curved slickenlines are available (e.g., Twiss and Gefell, 1990; Twiss et al., 1991). Roto-translational faults can be planar or listric (referred in Marshak and Mitra, 1988; Feng et al., 2016a,b) and can be numerous in specific terrains (Nevin, 1949).

Listric faults, on the other hand, have classically been presented implicitly in structural geology text mostly to be dip-slip normal faults (e.g., Fossen 2016; Blue Mountain Fault, Australia: Mackenzier (1993); field and numerical models: Hjelle 2014). However, I. strike-slip and II. oblique-slip listric faults have also been reported cursorily in the literature. For example, I. strike-slip listric faults have been reported in mega-scale from both the continental and oceanic crusts: at the releasing bend at the Loreto basin (Dorsey et al., 1995), ridge basin (Baratoux et al., 2011; Feng et al., 2018a), southern California (May et al., 1993), Loma Prieta bend in the San Andreas Fault (Dietz and Ellsworth, 1990; Tearpock and Bischke, 2002), the pull-apart Bhima basin (south India) (Dey, 2015), the boundary between Eurasian continental crust and Pacific oceanic crust (Taiwan Petroleum Exploration Division Chinese Petroleum Corporation, 1992), the Brevard fault zone

* Corresponding author.
E-mail address: soumyajitm@gmail.com (S. Mukherjee).

https://doi.org/10.1016/j.marpetgeo.2019.04.024
Received 5 January 2019; Received in revised form 6 April 2019; Accepted 18 April 2019
Available online 26 April 2019

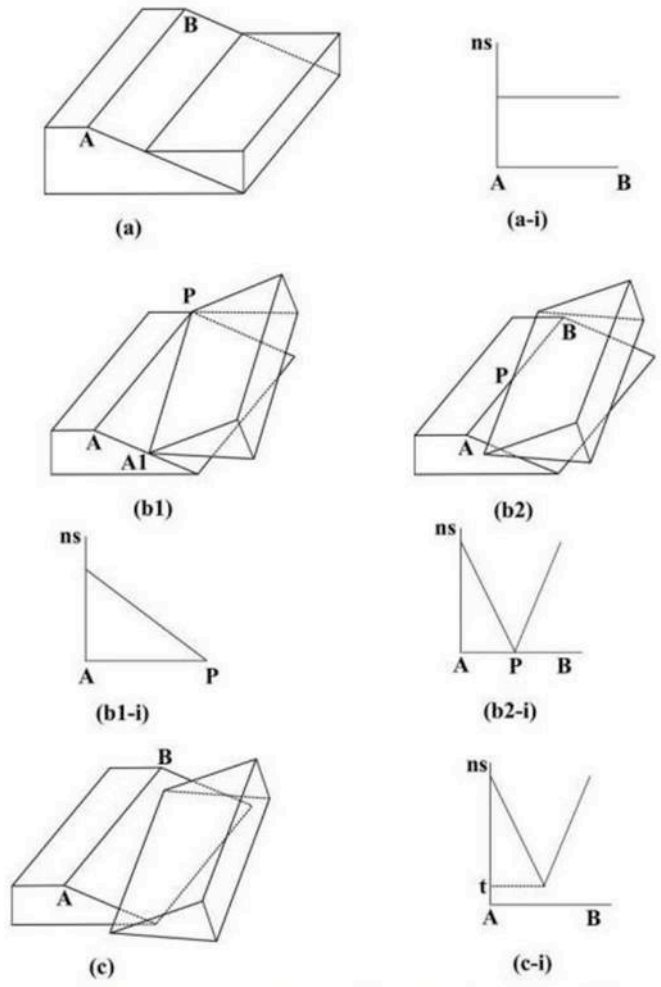

Fig. 1. Ideal faults. **a.** Translational normal fault. **a-i.** Net-slip (ns) is constant. **b1-b2.** Pure rotational fault. **b1-i**. Net-slip is zero at P and highest at A. **b2-i**. Net-slip is zero at p and highest at A and B. **c.** Roto-translational fault. **c-i.** Its net-slip profile. Reproduced from Fig. 1 of Mukherjee and Khonsari (2017).

(southern Appalachians) (Vauchez, 1987), to name a few. Rodgers and Chinnery (1969) describe strain and displacement patterns for strike-slip faults but do not simulate stretching lineation geometries on them. II. Oblique slip listric faults (Rep. Fig. 2) have been briefly reported from the North Minwun Basin (Mayanmar) (Morley, 2017), the eastern margin of the Dagg ridge (New Zealand) (Keary et al., 2013). Seminoe Mountans (U.S.) (Bergh and Snoke, 1992), the San Andreas fault zone (Seeber and Armbruster, 1995; Rust, 1998), syn-sedimentary slide from the Waitemata basin (New Zealand) (Sporli and Rowland, 2007), half-graben structures (Jayko and Bursik, 2012), the 12-May-2008 Sichuan seismicity in China (Zhang et al., 2010: high-angle reverse fault), the pop-up structures (Nabavi et al., 2017) etc. Unlike these authors, Claypool et al. (2002) describe a palm tree-like network of oblique-slip listric faults from Fiordland (New Zealand).

Besides merely reported (Marshak and Mitra, 1988), quantification of curvature of listric faults does not exist in the structural geological and the tectonic literature till date. Davis et al. (2019) discuss recently the kinematics of listric faults in 3D. While they describe how shear fractures are associated with such faults, the lineation pattern developed on the listric faults has not been explained.

Rotational/roto-translational faults are associated with hydrocarbon reserves (Michelsen and Andersen, 1982; Afifi et al., 2016) and landslides (e.g., Geist, 2000). Stability of structural hydrocarbon reserves depends on the faults that define them (Neil et al., 1993). Stability of a slope would depend presumably on the "ω/v" ratio of the fault that initiates its slide. Therefore, understanding the kinematics of such faults will be of great importance.

This article has two parts. A. Kinematic analysis of roto-translational faults with planar and curvi-planar/listric fault surfaces. This is achieved by modeling the loci of slickenside developed on such planar fault planes for specific ratios of rotation rate to the translation rate (ω/v) of the faulted blocks. The simulated curves are then correlated with the field-photographs of curved slickensides. Field works by the first author over last 20 years did not find good examples of curved slickensides from Indian terrains. So we chose previous authors' published photographs for the present work. B. For different ratios of "ω/v", geometries of slickenslides on curved fault planes are also simulated. Since curved lineations on curved fault planes have merely been reported, but no images are available, the curved that we simulate in ideal cases remain uncorrelated with the natural examples.

2. Curved slickensides and fault block rotation (rates)

Twiss and Gefell (1990) describe basic kinematics of curved slickenfibres (a kind of slickenlines). However, they do not estimate the rotation rate with respect to the translational velocity. Kusky et al. (1997) report up to 55^0 of curvature of the lineation on fault plane. A review of literature indicates that co-seismic faulting can produce curved slickenlines (e.g., Fig. 12 in Liu-Zeng et al., 2010), but exceptions do exist (Fig. 6b in Pan et al., 2014). Otsubo et al. (2013) report the most strikingly curved slickenside on fault plane related to the 11-April-2011 Mw = 6.8 earthquake from the Iwaki city (Japan). On the other hand, Pan et al. (2014) report a gently curved co-seismic striations on fault planes (their Fig. 6b) as a result of 12-May-2008 Mw = 7.9 seismicity in Wenchun (China).

Slip rates for translational faults of various types have been deduced, which usually range from a few mm- (Papanikolaou et al., 2005: using paleoseismologic throw-rate data from trenches and scarp profiles) up to a few cm per year (Kohn et al., 2004: based on *in-situ* Th–Pb dating of monazite). Mukherjee' and Khonsaris (2018) literature survey in their Table 1 reports a maximum rotation rate of crustal block $40^0\,Ma^{-1}$ from North Iceland volcanic rift zone. Paleomagnetic studies have revealed considerable rotation and rotation rates from several terrains (review in Table 1). However, from these places, curved slickensides have not been reported. Price and Scott (1994) provide a much reduced rate of rotation of $3^\circ\,Ma^{-1}$ from SW Turkey, a different terrain, due to inherent local tectonics. Horst et al. (2018) recently report a pronounced rotation of the crustal block up to 105° from the Húsavík-Flatey Fault (Iceland). Nur et al. (1989) described the tectonic reasons for significant variation of rotation rate of crustal blocks in different parts of the Earth.

3. Model

3.1. Planar fault planes

We model the geometries of curved slickenslides developed at different ratios of angular (ω) to linear velocities (v) of the faulted blocks using the programming software RStudio (Version 1.0.153-2009-20017). While the angular velocity represents the rotational component of faulting, the linear velocity denotes that for the translational component of movement between the two faulted blocks. The modeled curves generated were then fitted with already published 10 good quality field photographs of planar fault planes with prominent curved

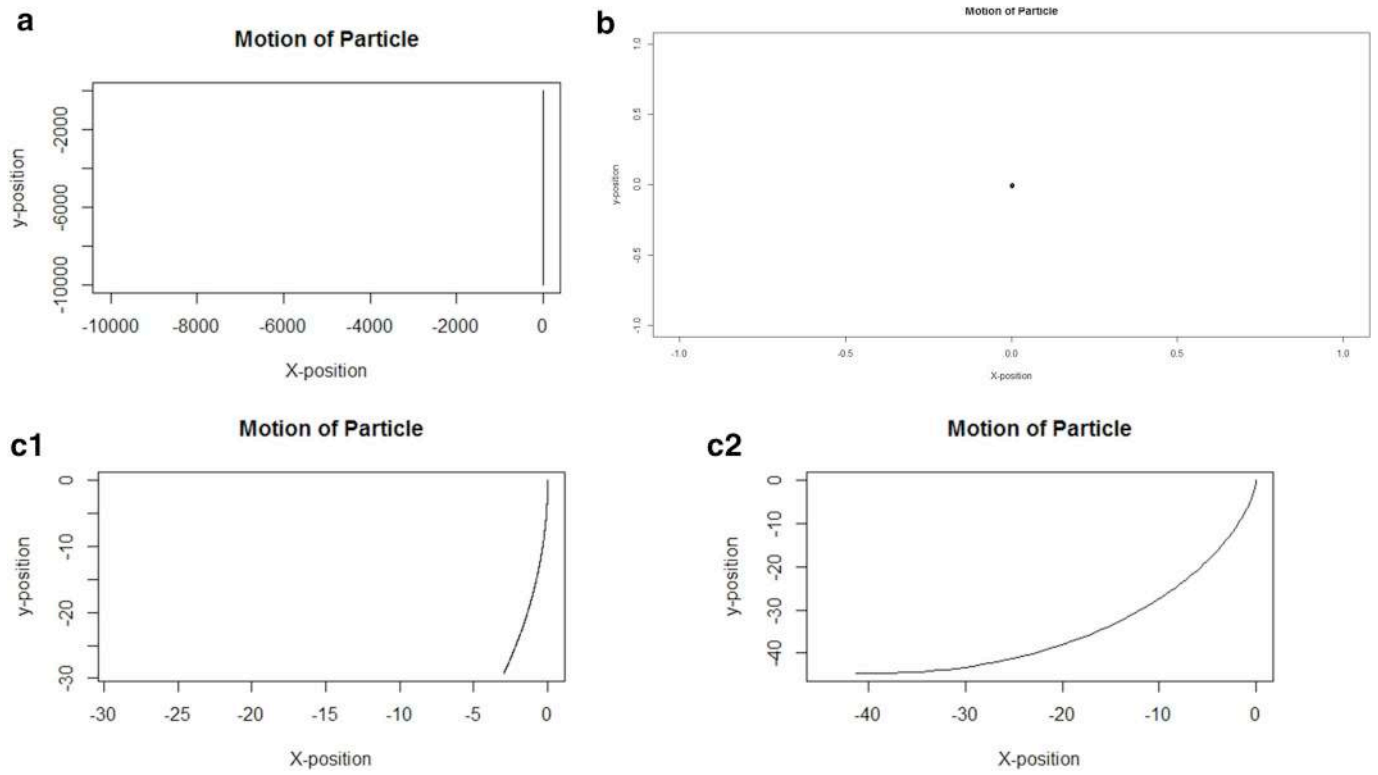

Fig. 2. The modeled lineation geometries on planar fault planes in various simple cases. **a.** ω = 0 case, for translational faults such as Fig. 1a. **b.** v = 0 case, for rotational faults such as Fig. 1b1-i. **c1.** ω ≠ 0, v ≠ 0 case (here ω/v = 1.3), for roto-translational faults, such as Fig. 1c. **c2.** ω ≠ 0, v ≠ 0 case (here ω/v = 5.6), for roto-translational faults, such as Fig. 1c.

(non-circular) slickensides (Table 2), using the Rhinoceros curve-fitting software (version 6 SR9 6.9.18271.20591). By finding the best fit, the "ω/v" ratios are deduced in each cases. We could not use each and every example of curved lineations from already published figures, as in some cases the slickenlines appear to have developed on gently curvilinear surfaces, such as Fig. 3 of Tapsoba and Howard (2017).

In the first part of this study, we have analyzed lineations that have developed on planar fault surfaces. In three simple tests, the model is found to match the common sense. To cross-check whether the RStudio-derived graphs (code in Appendix 1) gave realistic results, first, when we choose ω/v = 0, i.e., ω = 0 and v ≠ 0, a linear slickenside is simulated (Fig. 2a). This is the case of a purely translational fault (Fig. 1a). Second, when we take ω/v as "undefined", i.e., v = 0 (such as Fig. 1b1), the slickenside appears as merely a point (Fig. 2.b). Since v = 0, the point does not translate to attain a linear geometry, rather it only rotates about itself. Third, higher the ω/v magnitude, more curved is the slickenside. For example, compare the curve in Fig. 2.c1 which is having less curvature than that in Fig. 2c2, where ω/v are 1.3 and 5.6, respectively. The lineation geometries simulated in the work remain the same for normal, reverse and strike slip movement of the translational component of faulting.

The model curves produced by RStudio (sub-figures c in Fig. 3 and Rep. Figs. 3–11).The Rhinoceros curve-fitting software was used to find the correlation coefficient (R) between the traces of lineations (sub-figures d in Fig. 3 and Rep. Figs. 3–11 and The results viz., the "ω/v" ratio and the R values are presented against the corresponding slickenslides in Table 1.

3.2. Curved fault planes

In the second part of this work, the software Matlab (Version 9.3, 2017) was used to simulate the geometry of the lineations in 3D developed on listric fault planes that are perfectly spherical (Appendix-2). Fig. 4 presents such a lineation pattern when the hanging wall block moves with respect to the footwall block along a specific geographic direction with a constant speed (represented also by "v" in this work so that one can compare this with the previous case of "constant velocity"). Since the faulted block slides past along a curved surface, using the term "*constant velocity*" would be inappropriate. Fig. 5 represents the lineations for a perfect rotational movement of the faulted block. Fig. 6 represents the lineation geometry when ω = 0. Note the lineation in this case is a segment of a circle, as expected. Rep. Figs. 12 to 22 are the several cases of lineations produced by different "ω/v" magnitudes. As no published photographs of lineations exist on spherical listric fault planes till date to our knowledge, correlating them with the natural examples is indeterminate.

4. Discussions and conclusions

We simulate lineation pattern on planar and curviplanar fault planes for different ratios of rates of rotation and translation (ω/v) of the faulted blocks. With the computer codes, such ratios from field photographs of fault planes containing slickenslides can be obtained and their tectonic implications can be interpreted. For example, if one ignores the rotational component of fault blocks and apply Anderson's theory of faulting to decipher the principal stress orientations, it will be just an

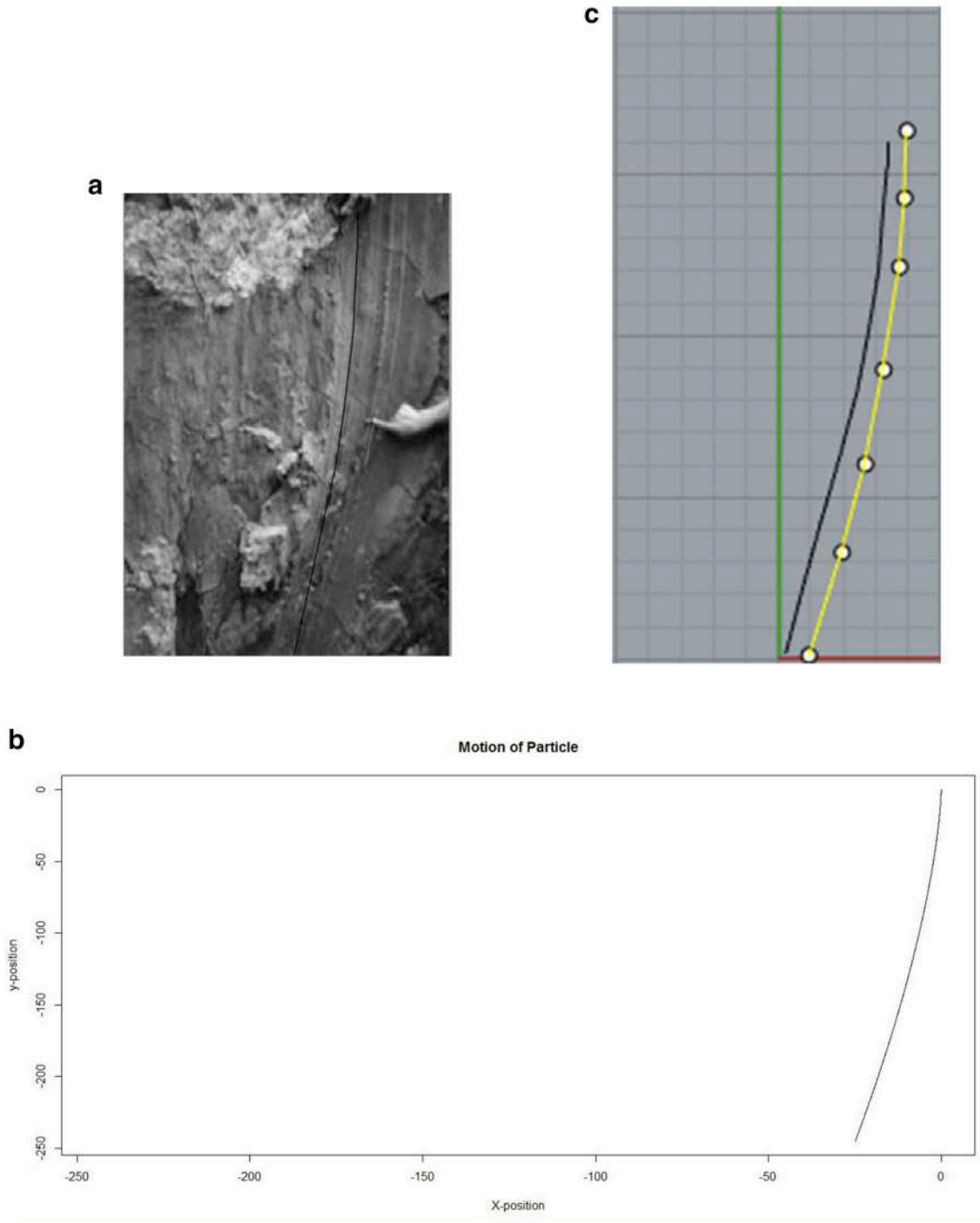

Fig. 3. a. Natural lineations on a fault plane from the Wenchuan region (China; Liu-Zhang et al., 2010; vide Table 1). Trace of the natural lineation is drawn. **b.** The modeled lineation for specific magnitudes of "ω/v" ratio, obtained by using the RStudio (Version 1.0.153-2009-20017). Here the units along X- and Y-axes represent the distances in a 1:1 scale. **c** Fit between curves in the sub-figure **b** and the sub-figure **c**. Vide code in Appendix 1.

approximation, and will be an imperfect interpretation. Analysis of the previously published images reveals the ω/v variation from 0.2 (San Miguelito range, Central México) to 2.4 (Hyogoken-Nambu, Japan).

Different kinds of linear marks can develop on fault planes (review in Resor and Meer, 2009). Such marks picked up in seismic images, known as corrugations, may not indicate slip direction of the fault (Ferrill et al., 1999). Therefore, those marks published by previous authors were avoided in analyzing in this study.

This second part of this work considers spherical geometry of the listric fault plane. Modeling listric fault surface in terms of a well known curve or surface is commonplace in structural geological/ seismicity related analyses (e.g., Archuleta and Brune, 1975). For example, Schultz (1987) numerically model the genesis of the listric strike-slip faults by considering circular arc-shaped curved fault planes for simplistic analyses and relate curvature of fault planes and their slip amounts. Schultz (1992) describes mechanics of listric faults in 2D. For

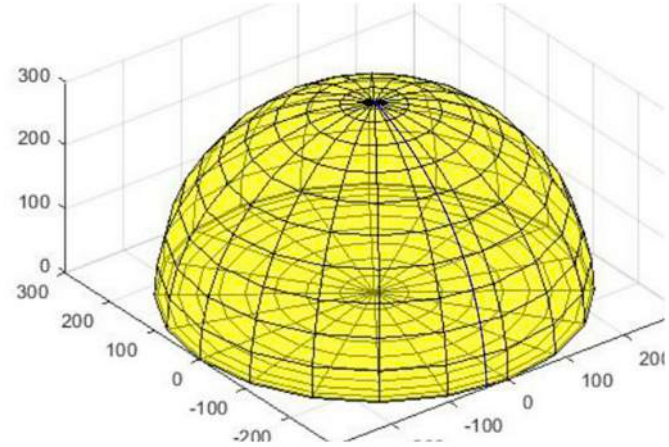

Fig. 4. Curved slickenside on a part of a spherical surface with radius = 200 units. ω = 1 unit per unit time.

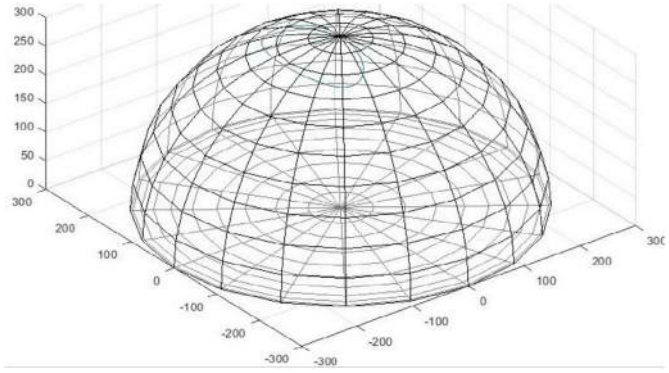

Fig. 5. Curved slickenside (blue-coloured) with perfect rotational motion on a part of a spherical surface with radius = 200 units. Radius of sphere 300 unit, ω = 3 units per unit time. The X-, Y- and the Z-axes are the dimensions in three directions using which the sphere is drawn.

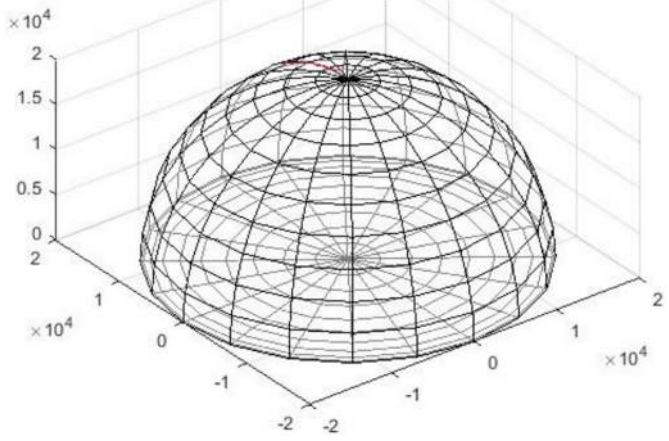

Fig. 6. The purpose of this figure is to demonstrate the lineation geometry when ω = 0 on a part of a spherical surface with radius = 20000 units. We chose a radius in this cae much more than that in Fig. 5 in order to observe the curved lineation at a higher resolution. Here the lineation generated (red-coloured) is the segment of a circle.

the sake of simplicity, his model considers the fault plane to be a circular arc. Mukherjeem and Agarwal (2018) consider circular fault plane in their 2D model of listric fault-induced shear heating. Ellis and McClay (1988) and Lohr et al. (2008) also presume cylindrical geometry of the fault plane while modeling listric fault kinematics.

However, rarely a parabolic fault plane is also considered in seismicity-related modeling (Griffin and Davies, web reference). A parabolic/paraboloid slip surface sounds mechanically feasible since such a geometry of the slip surface has been deduced from Mohr-Coulomb failure criteria in slop-stability studies (e.g., Wriggers et al., 1990). If the fault plane in 3D is not perfectly spherical and the 3D coordinates of its surface are known then such set of coordinates can be input in the Matlab program. Subsequently the lineations pattern for the different magnitudes of "ω/v" can also be obtained.

5. Model limitations

The natural faulting process can be more complicated than the "block models" shown in Billings (1954), which we follow in this work. At least seven issues are there. First, in block models, the faulted blocks are rigid, therefore the nature (magnitude and direction) of net slip is uniform along the fault trend. However, in reality, *(i)* a regional fault can change the slip pattern along its length, from thrust slip to oblique-slip (Gorum and Carranza, 2015); and *(ii)* the fault slip is maximum usually at the middle portion of the fault length and decreases (uniformly) towards the two tips (Ron et al., 1984; Feng et al., 2016b, 2018a,b; Fossen, 2016). These mean that the faulted blocks, in a regional-scale act as deformable solids. Second, Amos et al. (2007) report listric reverse faults from the Mackenzie Basin, New Zealand. When listric faults form a network (Claypool et al., 2002), the kinematics is expected to be more complicated. Third, faults with rotation components in their slip have been cursorily referred to have temporally shifting pivot of rotation (Billings, 1972). Fourth, Pueyo et al. (2002) deduce from paleomagnetic studies from the External Sierras (Southern Pyrenees) an acceleration in rotation rate of faulted blocks, from 5.5 to 9° Ma^{-2}. A ten times temporal increase of rotation rate has also been reported by Mochales et al. (2012) that has been linked with the emplacement of a thrust sheet. Fifth, A few natural faults have been reported where the geometries of curved lineations on the fault planes vary (e.g., Rep. Fig. 24). This means that over the same fault plane, "ω/v" ratio can change. Sixth, curvature of fault planes may vary temporally (McClay and Ellis, 1987). Seventh, Landslides and glacial abrasion sometimes leave curved lineations on (curved) planes. We have *not* dealt fault networks, shifting pivot, accelerated rotation of fault-blocks, different "ω/v" ratio at different portions of the faulted block, changing curvature of fault planes, and landslide and glacier-related lineations in this work.

Acknowledgements

This work is a part of Lokesh Tayade's Masters thesis. SM thanks his Ph.D. students Narayan Bose and Dripta Dutta for always assisting, even in their respective final years of thesis submission. A large number of geoscientists pointed out curved slickenslides from literature to SM, and we thank them all: Morgann Perrot, Willum M Dunne, Chrstine Regalla, Robert Twiss, Christoph Grützner, Janos Urai, Moraes Anderson, Gaël Lymer and Tom Raimondo. We apologize for missing any names. *SM collected published figures with curved lineations and wrote this article. LT ran codes and prepared the figures*. Constructive critical comments provided by Xiaojun Feng and an anonymous reviewers are thanked. Editorial handling by Adam Bumby is acknowledged. A further fault plane analysis (Mukherjee submitted) has been submitted to this journal. This work was funded by the CPDA grant of IIT Bombay provided to SM.

Table 1
Rotational information from different terrains in the world.

Author(s)	Locations	Rotation rate (^{0} Ma^{-1}) Total rotation (in^0)
Pueyo et al. (2002)	Thrust system in External Sierras (Southern Pyrenees)	5.3 to 21 At least 40
Mochales et al. (2012)	Thrust belt around Boltaña anticline, Southern Pyrenees	1 to 10 52
Rodriguez-Pinto et al. (2016)	Around Balzes anticline (Southern Pyrenees)	5.2
Oliva-Urcia and Pueyo (2007) and ref. therein	West of South Pyerenean Central Unit	25 to 50
Oliva-Urcia and Pueyo (2007) and ref. therein	Eastern part of South Pyerenean Central Unit	80
Oliva-Urcia and Pueyo (2007) and ref. therein	Internal Sierras, southwestern Pyrenees	08 to 26

Table 2
Numerical details of curve fitting exercise.

Sl. no.	Previous workers	Previous workers' fig. no.	Location (See Repository Fig. 1 for plot in the world map)	ω/v specified after curves were fitted	Fig. no. in this article	The correlation coefficient (the R-values)
1	Liu-Zang et al., (2010)	12	Hongkou (China)	0.6	Main text: 3a	0.96
2	Xu et al. (2013)	4a	San Miguelito range (México)	0.4	Repository: 3a	0.95
3	Xu et al. (2013)	4c	San Miguelito range (México)	0.2	Repository: 4a	0.95
4	Otsuki et al. (1997)	6a	Hyogoken (Japan)	1.4	Repository: 5a	0.95
5	Otsuki et al. (1997)	6b	Hyogoken (Japan)	2.4	Repository: 6a	0.95
6	Pan et al. (2014)	7c	Wenchuan (China)	0.6	Repository: 7a	0.96
7	Pan et al. (2014)	8d	Wenchuan (China)	0.4	Repository: 8a	0.96
8	Pan et al. (2014)	11c	Wenchuan (China)	0.2	Repository: 9a	0.95
9	Perrot (2013)	2.4 a	Appalaches (Quebec)	1.6	Repository: 10a	0.95
10	Singleton (2015)	4a	Metamorphic core complex, west-central Arizona (USA)	0.6	Repository: 11a	0.96

Appendix C. Supplementary data

Supplementary data related to this article can be found at https://doi.org/10.1016/j.marpetgeo.2019.04.024.

Appendix-1

The RStudio (Version 1.0.153-2009-20017) code:

```
radial_vel < - −0.05 #in m/unit_time
ang_vel < - −0.01 # in rad/unit_time ### One can, in general, have these as functions of t
t < - 0
x < - c (0)
y < - c (0)
steps < − 1000
step_size < − 0.01
for (i in 1:steps){
t < - t + step_size
x < − c (x,x [i]- 0.5*radial_vel*cos (ang_vel*t-pi/2))
y < − c (y,y [i]-radial_vel*sin (ang_vel*t-pi/2))
}
plot (x,y,main = "Motion of Particle"
xlab = "X-position", ylab = "y-position",
xlim = c (min(y),0), ylim = c (min(y), max(y)),
type = "l")
z = sqrt (30Ô2 - x̂2 - ŷ2)
```

Appendix-2

The general Matlab program to produce lineations on spherical surfaces:

```
[x,y,z] = sphere (20);
R = 300;
xEast = R * x;
yNorth = R * y;
zUp = R * z;
zUp(zUp < 0) = 0;
figure ('Renderer','opengl')
surf (xEast, yNorth, zUp,'FaceColor','yellow','FaceAlpha',0.5)
axis equal
hold on
z_p = [];
y_p = [];
x = [];
plot3 (x,y_p,z_p)
```

References

Afifi, A.S., Moustafa, A.R., Helmy, H.M., 2016. Fault block rotation and footwall erosion in the southern Suez rift: implications for hydrocarbon exploration. Mar. Petrol. Geol. 76, 377–396.

Amos, C.B., Burbank, D.W., Nobes, D.C., Read, S.A.L., 2007. Geomorphic constraints on listric thrust faulting: implications for active deformation in the Mackenzie Basin, South Island, New Zealand. J. Geophys. Res. 112, B03S11.

Archuleta, R.J., Brune, J.N., 1975. Surface strong motion associated with a stick-slip event in a foam rubber model of earthquakes. Bull. Seismol. Soc. Am. 65, 1059–1071.

Baratoux, L., Metelka, V., Naba, S., Jessell, M.W., Grégoire, M., Ganne, J., 2011. Juvenile Paleoproterozoic crust evolution during the Eburnean orogeny (~ 2.2–2.0 Ga), western Burkina Faso. Precambrian Res. 191, 18–45.

Bergh, S.G., Snoke, A.W., 1992. PolyphaseLaramide deformation in the shirley mountains, south-central Wyoming foreland. Mt. Geol. 29, 85–100.

Billings, M.P., 1954. Structural Geology, second ed. Prentice-Hall, New York 514 pp.

Billings, M.P., 1972. Structural Geology, third ed. Prentice-Hall of India Pvt. Ltd, pp. 178.

Claypool, A.L., Klepeis, K.A., Dockrill, B., Clarke, G.L., Zwingmann, H., Tulloch, A., 2002. Structure and kinematics of oblique continental convergence in northern Fiordland, New Zealand. Tectonophysics 359, 329–358.

Dasgupta, S., Mukherjee, S., 2017. Brittle shear tectonics in a narrow continental rift: asymmetric non-volcanic Barmer basin (Rajasthan, India). J. Geol. 125, 561–591.

Davis, T., Healy, D., Rivalta, E., 2019. Slip on wavy frictional faults: is the 3rd dimension a sticking point? J. Struct. Geol. 119, 33–49.

Dey, S., 2015. Geological history of the Kaladgi-Badami and Bhima basins, south India: sedimentarion in a Proterozoic intracratonic setup. In: Mazumder, R., Eriksson, P.G. (Eds.), Precambrian Basins of India: Stratigraphic and Tectonic Context. vol. 43. Geol. Soc., London, Mem, pp. 283–296.

Dietz, L.D., Ellsworth, W.L., 1990. The October 17, 1989, Loma Prieta, California, earthquake and its aftershocks: geometry of the sequence from high-resolution

locations. Geophys. Res. Lett. 17, 1417–1420.
Doblas, M., 1998. Slickenside kinematics indicators. Tectonophysics 295, 187–197.
Doblas, M., Mahecha, V, Hoyos, M, Lopez-Ruiz, J., 1997. Slickenside and fault surface kinematic indicators on active normal faults of the Alpine Betic cordilleras, Granada, southern Spain. J. Struct. Geol. 19, 159–170.
Dorsey, R.J., Umhoefer, P.J., Renne, P.R., 1995. Rapid subsidence and stacked gilbert-type fan deltas, pliocene Loreto basin, baja California sur, Mexico. Sediment. Geol. 98, 181–204.
Ellis, P.G., McClay, K.R., 1988. Listric extensional fault systems – results from analogue model of experiments. Basin Res. 1, 55–70.
Feng, X., Jessel, M.W., Amponsah, P.O., Martin, R., Ganne, J., Liu, D., Batt, G.E., 2016a. Effect of strain weakening on Oligocene-Miocene self organization of the Australian-Pacific plate boundary fault in southern New Zealand: insights from numerical modelling. J. Geodyn. 100, 130–143.
Feng, X., Amponsah, P.O., Martin, R., Ganne, J., Jessel, M.W., 2016b. 3D numerical modelling of the influence of pre-existing faults and boundary conditions on the distribution of deformation: example of northwestern Ghana. Precambrian Res. 274, 161–179.
Feng, X., Wang, E., Ganne, J., Amponsah, P., Martin, R., 2018a. Role of volcano-sedimentary basins in the formation of greenstone-granitoid belts in the west african craton: a numerical model. Minerals 8, 73.
Feng, X., Wang, E., Ganne, J., Martin, R., Jessell, M., 2018b. The exhumation along the Kenyase and Ketesso shear zones in the Sefwi terrane, West African Craton: a numerical study. Geosci. J. 1–18.
Ferrill, D.A., Stamatakos, J.A., Sims, D., 1999. Normal fault corrugation: implications for growth and seismicity of active normal faults. J. Struct. Geol. 21, 1027–1038.
Fossen, H., 2016. Structural Geology, second ed. Cambridge University Press ISBN-13: 978-1107057647.
Geist, E.L., 2000. Origin of the 17 july 1998 Papua New Guinea Tsunami: earthquake or landslide. Seismol Res. Lett. 71, 344–351.
Gorum, T, Carranza, EJM., 2015. Control of style-of-faulting on spatial pattern of earthquake-triggered landslides. J. Environ. Sci. Technol 12, 3189–3212.
Griffin, J.Davies, G. Internet Reference. Earthquake Sources of the Australian Plate Margin. Revised Models for the 2018 National Tsunami and Earthquake Hazard Assessments. https://data.gov.au/dataset/earthquake-sources-of-the-australian-plate-margin-revised-models-for-the-2018-national-tsunami- Accessed on 04-Dec-2018.
Hjelle, Ø., 2014. A Hamilton–Jacobi Framework for Modelinggeological Folding and Deformation. pp. 80–88 Ph.D. thesis.
Horst, A.J., Karson, J.A., Varga, R.J., 2018. Large rotations of crustal blocks in the Tjörnes fracture zone of northern Iceland. Tectonics 37, 1607–1625.
Jayko, A.S., Bursik, M., 2012. Active Transtensional intracontinental basins: M Walker Lane belt. In: Busby, C., Azor, A. (Eds.), Tectonics of Sedimentary Basins: Recent Advances. Wiley-Blackwell, pp. 226–248.
Keary, P., Klepeis, K.A., Vine, F.J., 2013. Global Tectonics, third ed. Wiley-Blackwell978-1-4051-0777-8.
Kohn, M.J., Wieland, M.S., Parkinson, C.D., Upreti, B.N., 2004. Miocene faulting at plate tectonic velocity in the Himalaya of central Nepal. Earth Planet. Sci. Lett. 228, 299–310.
Kusky, T.M., Bradley, D.T., Haeussler, P., 1997. Progressive deformation of the Chugach accretionary complex, Alaska, during a paleogene ridge-trench encounter. J. Struct. Geol. 19, 139–157.
Liu-Zeng, J., Wen, L., Sun, J., Zhang, Z., Hu, G., Xing, X., Zeng, L., Xu, Q., 2010. Surficial slip and rupture geometry on the beichuan fault near Hongkou during the Mw 7.9 Wenchuan earthquake, China. Bull. Seismol. Soc. Am. 100, 2615–2650.
Lohr, T., Krawczyk, C.M., Oncken, O., Tanner, D.C., 2008. Evolution of a fault surface from 3D attribute analysis and displacement measurements. J. Struct. Geol. 30, 690–700.
Mackenzier, D.E., 1993. Geology of the Featherbed Cauldron Complex. In: Queensland: Part 1-Eruptive Rocks and Post-Volcanic Sediments. Australian Geological Survey Organization, North0 642 19861 6, .
McClay, K.R., Ellis, P.G., 1987. Generation of extensional fault systems developed in model experiments. Geology 15, 341–344.
Mandal, N., Chakraborty, C., 1989. Fault motion and curved slickenlines: a theoretical analysis. J. Struct. Geol. 11, 497–501.
Marshak, S., Mitra, G., 1988. Basic Methods of Structural Geology. Prentice Hall.
May, S.R., Ehman, K.D., Gray, G.G., Crowell, J.C., 1993. A new angle on the tectonic evolution of the Ridge Basin, a “strike-slip” basin in Southern California. Geol. Soc. Am. Bull. 105, 1357–1372.
Michelsen, O., Andersen, C., 1982. Mesozoic structural and sedimentary development of the Danish Central Graben. In: Kaasschieter, J.P.H., Reijers, T.J.A. (Eds.), Petroleum Geology of the Southeastern North Sea and the Adjacent Onshore Areas. The Hague, pp. 93–102 ISBN-13 978-94-010-8942-5.
Mochale, T., Casas, A.M., Pueyo, E.L., Barnolas, A., 2012. Rotational velocity for oblique structures (Boltaña anticline, Southern Pyrenees). J. Struct. Geol. 35, 2–16.
Morley, C.K., 2017. Syn-kinematic sedimentation at a releasing splay in the northern Minwun Ranges, Sagaing Fault zone, Myanmar: significance for fault timing and displacement. Basin Res. 29, 684–700.
Mukherjee, S., 2014. Atlas of Shear Zone Structures in Meso-Scale. Springer Geology, Cham, pp. 1–124 ISBN 978-3-319-0088-6.
Mukherjee, S., 2015. Atlas of Structural Geology. Elsevier, Amsterdam978-0-12-420152-1.
Mukherjee, S., 2018. Moment of inertia for rock blocks subject to bookshelf faulting with geologically plausible density distributions. J. Earth Sys. Sci. 127, 80.
Mukherjee S. Submitted. Particle tracking in ideal faulted blocks using 3D co-ordinate geometry. Mar. Petrol. Geol.
Mukherjeem, S., Agarwal, I., 2018. Shear hear heat model for gouge free dip-slip listric normal faults. Mar. Petrol. Geol. 98, 397–400.
Mukherjee, S., Khonsari, M.M., 2017. Brittle rotational faults and the associated shear heating. Mar. Petrol. Geol. 88, 551–554.
Mukherjee, S., Khonsari, M.M., 2018. Inter-book normal fault-related shear heating in brittle bookshelf faults. Mar. Petrol. Geol. 97, 45–48.
Nabavi, S.T., Alavi, S.A., Mohammadi, S., Ghassemi, M.R., Frehner, M., 2017. Analysis of transpression within contractional fault steps using finite-element method. J. Struct. Geol. 96, 1–20.
Neil, J.T., Magorian, T.R., Byrne, K.O., Denzier, S., 1993. Strategic Petroleum Reserve (SPR), Additional Geologic Site Characterization Studies. Bayou Choctaw Salt Dome, Louisiana. Albuquerque up to D2.
Nevin, C.M., 1949. Principles of Structural Geology. John Wiley & Sons, New York, pp. 88.
Nur, A., Ron, H., Scott, O., 1989. Mechanics of distributed fault and block rotation. In: Kissel, C., Laj, C. (Eds.), Paleomagnetic Rotations and Continental Deformation. Kluwer Academic Publishers, pp. 209–228.
Oliva-Urcia, B, Pueyo, EL., 2007. Rotational basement kinematics deduced from re-magnetized cover rocks (Internal Sierras, southwestern Pyrenees). Tectonics 26, TC4014.
Otsubo, M., Shigematsu, N., Imanishi, K., Ando, R., Takahashi, M., Azuma, T., 2013. Towards slip change based on curved slickenlines on fault scarps along Itozawa fault caused by 2011 Iwaki earthquake, northeast Japan. Tectonophysics 608, 970–979.
Otsuki, K., Minagawa, J., Aono, M., Ohtake, M., 1997. On the curved striations of nojima seismic fault Engraved at the 1995 Hyogoken-nambu earthquake, Japan. J. Seismol. Soc. Japan 49, 451–460.
Pan, J., Li, H., Si, J., Pei, J., Fu, X., Chevalier, M.-L., Liu, D., 2014. Rupture process of the Wenchuan earthquake (Mw 7.9) from surface ruptures and fault striations characteristics. Tectonophysics 619–620, 13–28.
Papanikolaou, I.D., Roberts, G.P., Michetti, A.M., 2005. Fault scarps and deformation rates in Lazio–Abruzzo, Central Italy:Comparison between geological fault slip-rate and GPS data. Tectonophysics 408, 147–176.
Perrot, M., 2013. Étude Structuraleet Microstructurale de la Faille St-Josephetde la lignebaie Vertebromptondans les Appalaches du suddu Québec. University of Quebec in Montreal, pp. 30 Master of Earth Science Thesis.
Price, S.P., Scott, B., 1994. Fault block rotations at the edge of a zone of continental extension; southwest Turkey. J. Struct. Geol. 16, 381–392.
Pueyo, E.L., Millan, H., Pocovi, A., 2002. Rotation velocity of a thrust: a paleomagnetic study in the External Sierras (southern Pyrenees). Sediment. Geol. 146, 191–208.
Resor, P.G., Meer, V.E., 2009. Slip heterogeneity on a corrugated fault. Earth Planet. Sci. Lett. 288, 483–491.
Rodgers, D.A., Chinnery, M.A., 1969. The displacements and strains associated with a curved strike-slip fault. Eos, Trans., Am. Geophys. Union 50, 238.
Rodriguez-Pinto, A., Pueyo, E.L., Calvin, P., Sanchez, E., Ramajo, J., Casas, A.M., Ramon, M.J., Pocovi, A., Barnolas, A., Roman, T., 2016. Rotational kinematics of a curved fold: the Balzes anticline (Southern Pyrenees). Tectonophysics 677–678, 171–189.
Ron, H., Freund, R., Garfunkel, Z., Nur, A., 1984. Block rotation by strike-slip faulting: structural and paleomagnetic evidence. J. Geophys. Res.: Solid Earth 89 (B7), 6256–6270.
Rowland, J.V., Sibson, R.H., 2001. Extensional fault kinematics within the Taupo Volcanic Zone, New Zealand: soft-linked segmentation of a continental rift system. N. Z. J. Geol. Geophys. 44, 271–283.
Rust, D., 1998. Contractional and extensional structures in the transpressive 'Big Bend' of the San Andreas fault, southern California. In: Holdsworth, R.E., Strachan, R.A., Dewey, J.E. (Eds.), Continental Transpressional and Transtensional Tectonics. vol. 135. Geol. Soc., London, Spec. Publ., pp. 119–126.
Schultz, R.A., 1992. Mechanics of curved slip surfaces in rock. Eng. Anal. Bound. Elem. 10, 147–154.
Schultz, R.A., 1987. Mechanics of Curved Strike-Slip Faults. Ph.D. thesis. Purdue University, pp. 1–142.
Seeber, L., Armbruster, J.G., 1995. The san Andreas fault system through the Transverse ranges as illuminated by earthquakes. J. Geophys. Res. 100, 8285–8310.
Singleton, J.S., 2015. The transition from large-magnitude extension to distributed dextral faulting in the Buckskin-Rawhide metamorphic core complex, west-central Arizona. Tectonics 34, 1685–1708.
Sporli, K.B., Rowland, J.V., 2007. Superposed deformation in turbidites and syn-sedimentary slides of the tectonically active Miocene Waitemata Basin, northern New Zealand. Basin Res. 19, 199–216.
Taiwan Petroleum Exploration Division, Chinese Petroleum Corporation, 1992. Petroleum Geology of Taiwan. pp. 27–29.
Tapsoba, B., Howard, W., 2017. Modeling the Geometry of Shear Zone Hosted Gold + Bismuth Telluride Bearing Quartz Veins at the Historic Bunker Hill Mine, South of Nelson, B.C.- a Covert , Mildly, Folded Tension Vein Array. Orogeny to Ore: Cordilleran Tectonics Workshops. University of British Coloumbia, pp. 88–90.
Tearpock, D.J., Bischke, R.E., 2002. Applied Sub-surface Geological Mapping with Structural Methods, second ed. Prentice Hall, New Jersey0-13-859315-9.
Twiss, R., Portzman, G.M., Hurst, S.D., 1991. Theory of slickenline patterns based on the velocioty gradient tensor and microrotation. Tectonophysics 186, 215–239.

Twiss, R.J., Gefell, M.J., 1990. Curved slickenfibers: a new brittle shear sense indicator with application to a sheared serpentinite. J. Struct. Geol. 12, 471–481. https://www.researchgate.net/profile/Jonathan_Griffin5/publication/328518053_Earthquake_sources_of_the_Australian_plate_margin_Revised_models_for_the_2018_national_tsunami_and_earthquake_hazard_assessments/links/5bd23715299bf1124fa36bab/Earthquake-sources-of-the-Australian-plate-margin-Revised-models-for-the-2018-national-tsunami-and-earthquake-hazard-assessments.pdf Accessed on 24-Nov-2018.
Vauchez, A., 1987. Brevard fault zone, southern Appalachians: a medium-angle, dextral, Alleghanian shear zone. Geology 15, 669–672.
Wriggers, P., Vu Van, T., Stein, E., 1990. Finite element formulation of large deformation impact-contact problems with friction. Comp. Struct. 37, 319–331.
Xu, S., Nieto-Samaniego, A.F., Alaniz-Alvarez, S.A., 2013. Origin of superimposed and curved slickenlines in San Miguelito range. Central México. Geol. Acta 11, 103–112.
Zhang, P.-Z., Wen, X.-z., Shen, Z.-K., Chen, J.-h., 2010. Oblique, high-angle, listric-reverse faulting and associated development of strain: the Wenchuan earthquake of May 12, 2008, sichuan, China. Annu. Rev. Earth Planet Sci. 38, 351–380.